Earthquake-swarms, slow-slip and fault-interactions at the western-end of the Hellenic Subduction System precede the M_w 6.9 Zakynthos Earthquake, Greece

Vasiliki Mouslopoulou[1,3*], Gian-Maria Bocchini[2], Simone Cesca[3], Vasso Saltogianni[3], Jonathan Bedford[3], Gesa Petersen[3], Michael Gianniou[4,5], Onno Oncken[3]

[1]National Observatory of Athens, Institute of Geodynamics, Athens, 11810, Greece (vasiliki.mouslopoulou@noa.gr)

[2]Ruhr University of Bochum, Institute of Geology, Mineralogy and Geophysics, Germany (Gian.Bocchini@rub.de)

[3]GFZ Helmholtz Centre Potsdam, German Research Centre for Geosciences, Telegrafenberg 14473 Potsdam, Germany (cesca@gfz-potsdam.de; salto@gfz-potsdam.de; jbed@gfz-potsdam.de; gesap@gfz-potsdam.de; oncken@gfz-potsdam.de)

[4] Hellenic Cadastre, Athens, 15562, Greece (mgianniu@ktimatologio.gr)

[5]University of West Attica, Athens, 12243, Greece (mgianniou@uniwa.gr)

*Corresponding author: Vasiliki Mouslopoulou (vasiliki.mouslopoulou@noa.gr)

Key Points:

- First ever report of slow-slip event in the Hellenic Subduction System prior to a M_w 6.9 event
- Synergy of upper-plate faulting, slow-slip & earthquake-swarms tectonically destabilise a subduction-termination prior to the mainshock
- Alternating phases of seismic and aseismic slip at various depths accommodates plate-motion at the western Hellenic Subduction System

Abstract

The month-to-year-long deformation of the Earth's crust where active subduction zones terminate is poorly explored. Here we report on a multidisciplinary dataset that captures the synergy of slow-slip events, earthquake swarms and fault-interactions during the ~5 years leading up to the 2018 M_w 6.9 Zakynthos Earthquake at the western termination of the Hellenic Subduction System (HSS). It appears that this long-lasting preparatory phase initiated due to a slow-slip event that lasted ~4 months and released strain equivalent to a ~M_w 6.3 earthquake. We propose that the slow-slip event, which is the first to be reported in the HSS, tectonically destabilised the upper 20-40 km of the crust, producing alternating phases of seismic and aseismic deformation, including intense microseismicity (M<4) on neighbouring faults, earthquake swarms in the epicentral area of the M_w 6.9 earthquake ~1.5 years before the main event, another episode of slow-slip immediately preceding the mainshock and, eventually, the large (M_w 6.9) Zakynthos Earthquake. Tectonic instability in the area is evidenced by a prolonged (~4 years) period of overall suppressed b-values (<1) and strong earthquake interactions on discrete strike-slip, thrust and normal faults. We propose that composite faulting patterns accompanied by alternating (seismic/aseismic) deformation styles may characterise multi-fault subduction-termination zones and may operate over a range of timescales (from individual earthquakes to millions of years).

Keywords: Hellenic subduction, slow-slip, upper-plate, microseismicity, Zakynthos, plate-interface

1 Introduction

Well-monitored examples of large-magnitude earthquakes that rupture subduction plate-boundaries reveal that these earthquakes may be preceded by episodes of slow-slip, swarm activity and/or large foreshocks (i.e. Kato et al., 2012; Bouchon et al., 2013; Schurr et al., 2014). Examples that document such interactions, most of which have been operating on the plate-interface, include the 2011 M_w 9 Tohoku-Oki Earthquake in Japan, the 2012 M_w 7.6 Nicoya Peninsula Earthquake in Costa Rica, and the 2014 M_w 8.1 Iquique megathrust earthquake in Chile (Kato et al., 2012; Schurr et al., 2014; Ruiz et al., 2014; Davis et al., 2015; Uchida et al., 2016). The interrelation, and possible interdependence, of these deformational processes is nevertheless poorly understood, especially in circumstances where upper-plate faulting accommodates a significant percentage of the plate-motion, with the plate-interface playing a secondary role (i.e. Wallace et al., 2012; Cesca et al., 2017). Such settings are often encountered at the terminations of subduction zones (Mouslopoulou et al., 2019), where plate-motion transitions from thrust to strike-slip faulting, producing complex kinematic patterns in the overriding plate (Mann and Frohlich, 1999). The characteristics (duration, size, distribution) of the interplay between the various types of deformation (seismic vs aseismic) along subduction terminations, especially prior or immediately after large-magnitude earthquakes, is poorly explored mainly due to the lack of relevant data.

The M_w 7.8 Kaikoura Earthquake, that ruptured the southern-end of the Hikurangi margin in 2016 (Cesca et al., 2017), to-date provides the only well-monitored example of a large-magnitude earthquake that ruptured a subduction termination (Mouslopoulou et al., 2019). This earthquake enhanced our understanding of seismogenesis along subduction terminations, as it demonstrated that earthquake-rupture involved primarily (~80%) slip on upper-plate faults, with only weak seismic-slip and aseismic afterslip on the plate-interface (Mouslopoulou et al., 2019).

On October 25th, 2018 a M_w 6.9 earthquake ruptured the western termination of the Hellenic Subduction System (HSS) across a zone where plate-motion transitions from mainly thrust to mainly strike-slip faulting (Royden and Papanikolaou, 2011), providing a valuable new case-study of a well-monitored earthquake that ruptures a subduction termination (Fig. 1). This earthquake, that occurred southwest of the island of Zakynthos (Sokos et al., 2020) (Fig. 1), was preceded by a 5-year-long tectonic instability in the broader epicentral area of the M_w 6.9 event and an intense aftershock sequence (Figs 2 and 3). Here, we report on a multidisciplinary dataset of seismological, geodetic, seismic-reflection and bathymetric information that, collectively, capture the earthquake and fault kinematics within this earthquake sequence (hereafter refer to as the Zakynthos Earthquake Sequence - ZES), prior to and after the main event. We find that alternating phases of aseismic and seismic deformation on the subduction-thrust and the overriding plate, respectively, preceded the M_w 6.9 event and accounted for at least 15% of the relative Eurasian/African plate-motion. The aftershock sequence was accommodated by thrust, strike-slip, and normal faulting in the upper-plate (<20 km) and accounted for ~75% of the plate convergence.

2 The kinematics of the western HSS and the M_w 6.9 Zakynthos Earthquake

In the eastern Mediterranean, the oceanic African Plate is being obliquely subducted along the Hellenic margin beneath the continental Eurasian Plate at rates ranging from ~ 26 to 34 mm/yr (McClusky et al., 2000) (Fig. 1). At its western-end the subduction system terminates against the dextral Kefalonia Transform Fault (Louvari et al. 1999; Sachpazi et al. 2000), transferring its relative plate-motion onto the Apulian collision front (Pérouse et al., 2017) (Fig. 1). The kinematic transition from nearly orthogonal convergence (in the south) to pure strike-slip (in the north) is accommodated, along a ~100 km wide zone offshore from western Peloponnese, by strike-slip, thrust and normal faulting (Fig. 1). The faults presented in Figure 1 are derived from a combination of published information (Kokinou et al., 2005; Kokalas et al., 2013; Makris and Papoulia, 2014; Wardell et al., 2014), analysis of bathymetric data (https://portal.emodnet-bathymetry.eu/?menu=19) and re-interpretation of four (Z207, KY301, Z151AB, KY311 and KY209; for location see Fig. 1) published Multi-channel seismic reflection profiles (Kokalas et al., 2013; Wardell et al., 2014) (Fig. 4).

Beneath western Peloponnese the top of the plate-interface lies at depths between 20-40 km and has an average dip of ~17° (Pearce et al., 2012; Halpaap et al., 2018, 2019) (Figs. 1 and 3). Just southwest of Zakynthos and proximal to the region of the 2018 mainshock, the plate-interface lies at ~15 km depth (Clément et al., 2000), with a series of east-dipping thrust faults displacing the upper section (<15 km) of the crust and the sea-bed (Louvari et al. 1999; Sachpazi et al. 2000; Wardell et al., 2004; Kokinou et al. 2005). Low-dipping reverse faulting in the area is also supported by moment tensors of instrumental seismicity (i.e. Anderson and Jackson, 1987). On the hangingwall of these thrust faults, numerous normal faults have been identified to displace post-Miocene deposits down to depths of at least 10 km (Kokalas et al, 2013; Wardell et al., 2014; this study) (Fig. 4).

The 2018 Zakynthos mainshock ruptured the upper <20 km of the crust as a result of shallow thrust and moderately dipping dextral strike-slip faulting (Haddad et al., 2020; Sokos et al., 2020). The focal mechanism presents a large non-double-couple (non-DC) component with a large negative CLVD indicating a complex rupture process (Sokos et al., 2020). The Global Centroid Moment Tensor (Global CMT) project suggests a centroid depth for this event of ~12 km and a total seismic-moment release of 2.32×10^{19} Nm (Dziewonski et al., 1981; Ekström et al., 2012). Three past earthquakes with sizes and focal mechanisms similar to that recorded in 2018, have ruptured the crust proximal to Zakynthos over the last ~60 years (in 1959, 1976 and 1997; http://bbnet.gein.noa.gr/HL/). The orientation of their focal mechanisms (Kiratzi and Louvari, 2003; Sokos et al., 2020) is in agreement with the plate-convergence (Fig. 1), indicating that these earthquakes accommodated a fraction of the relative African-Eurasian plate-motion. No events greater than M7 have been recorded in the ZES region instrumentally or historically (Papazachos and Papazachou, 2003).

3 The 2014-2019 Zakynthos Earthquake Sequence (ZES)

3.1 Sequence characteristics

The earthquake sequence analysed here (lon: 19.5°E to 21.6°E / lat: 36.8°N to 38°N) derives from the Hellenic Unified Seismological Network (HUSN; http://bbnet.gein.noa.gr/HL/) and includes data from the stations of the National Observatory of Athens (NOA), the University of Patras (UP), the Aristotle University of Thessaloniki (AUTH) and eight additional seismic stations deployed in western Peloponnese immediately after the mainshock. The ZES extends over an area of ~18,000 km^2, from northwest Peloponnese to the west of the islands of Zakynthos and Kefalonia (Figs 1 and 3), and spans a time-period of ~5 ½ years (January 1st, 2014 to May 31st, 2019) (Fig. 2a). The ZES includes >12,000 earthquakes (Table S3), with the largest event (M_w 6.9) having occurred ~40 km southwest of the island of Zakynthos on October 25th, 2018 (22:54 UTC) due to oblique-thrust faulting (Fig. 1; Table S4). About one third of the events in the ZES occurred prior to the mainshock while two thirds were aftershocks (Figs 2 and 3). The majority of these earthquakes have magnitudes below 3.5 (Fig. 2a). The magnitude of completeness (M_c) in the ZES prior to the mainshock is 2.0±0.1, it abruptly increases to 3.5 after the mainshock (Fig. 2b) while it returns to pre-mainshock values (~2.0) about 120 days after the mainshock (Fig. 2b).

The seismic-moment (M_0) release during the ZES has not been uniform (Fig. 2c). In addition to the energy released during the mainshock, two M>5 earthquakes that occurred on January 11th, 2014 (M_w 5.1) and on March 29th, 2016 (M_w 5.4) dominate the graph in Figure 2c. A further M_w 4.9 earthquake struck about 30 minutes before the mainshock (22:22 UTC); however, its seismic-moment is poorly resolved (Fig. 2c), as it is overprinted by the mainshock's moment release. The total M_0 released in the ~5 years prior to the mainshock is equivalent to a ~M5.8 earthquake, while the cumulative M_0 released during the entire ZES is equivalent to a ~M7 earthquake (Table S1).

Seismicity rates within the ZES also vary through time (Fig. 2c). For example, a 6-month interval of increased seismicity (September 2016 to April 2017) is preceded (December 2015 to August 2016) and followed (May 2017 to October 2018) by yearlong periods where the seismicity rates are lower, especially proximal to the epicentral area of the M_w 6.9 earthquake (Fig. 2a,c and Fig. S2). This swarm-like activity initiated ~1.5 years before the mainshock and is characterised by 3 times higher seismicity rates compared to the preceding and following time-periods, absence of a dominant earthquake at the start of the sequence, spatiotemporally clustered events in the proximity of the (future) mainshock location, and the largest (1.59) coefficient of variation (CV) during the ZES (Fig. 2c,d). These characteristics collectively indicate temporally clustered earthquake activity.

To assess whether these fluctuations in the seismicity rates reflect stress changes within the Earth's crust, we have calculated the evolution of the b-value of the Gutenberg-Richter frequency-magnitude distribution in the study area, from January 2013 to May 2019 (Fig. 2d and Fig. S1c). The b-value in a given area describes the relative abundance of small to large-magnitude earthquakes at that location and, thus, any temporal variation in b-values is often interpreted to reflect changes in the confining stress within the seismogenic crust (Schorlemmer et al., 2005). Namely, b-values have been found to relate inversely to differential stresses, with low (<1) b-values often indicating elevated stress while high (>1) b-values indicate low/heterogeneous stresses. Here, b-values were derived for subsets of 500 earthquakes with half-overlapping time-windows for the foreshock sequence (01.01.2013 to 25.10.2018) and for subsets of 1000 events in the aftershock sequence (for more details on the b-value calculation refer to Text S1 in the Supporting Information). We find that during the ~70 months preceding the mainshock, b-values in the ZES fluctuate over four main time-intervals (Fig. 2d and Fig. S1c): (i) from January 2013 to December 2014 the b-value is uniform and about 1 (0.94±0.09); (ii) from January 2015 to August 2016, the b-value drops significantly (as low as 0.81); (iii) from September 2016 to April 2017, there is a sharp increase in the b-values (up to 1.36) while (iv) from May 2017 till the mainshock (October 25th, 2018), the b-value drops again below 1 (average of 0.88±0.08). The mean b-value of the aftershock sequence is 1.18±0.12, in agreement with values from other aftershock sequences worldwide (Gulia et al., 2018). In summary, b-values in the ZES remained uniform and equal to ~1 during 2013 and 2014, while from early 2015 until the main-shock in late 2018 the b-values were overall <1, except for the 6-month time-period of the swarm-like activity (Fig. 2d). For a sequence such as the ZES, where multiple faults appear to be active simultaneously in the subsurface (Figs 1-4), earthquake relocation is vital, not only because it allows delineation of individual earthquake clusters with discrete faults (Waldhauser and Ellsworth, 2002) but also because it may help identify day-to-month long earthquake interactions between neighbouring faults (Mouslopoulou and Hristopulos, 2011).

3.2 Earthquake relocation

We successfully relocated 12,620 earthquakes that occurred within the ZES from 01.01.2014 until 31.05.2019 (Fig. 3), using a local minimum 1-D velocity model (Sachpazi et al., 2000) and manually picked P & S phase onsets determined at the National Observatory of Athens (NOA). The main challenges associated with the relocation arose from the large azimuthal gaps (average >180°) between the seismic source and the seismographs, the poor station density and the complex velocity structure of the study area (Karastathis et al., 2015). We used a constant Vp/Vs ratio of 1.80 in accordance with other seismological studies in the area (Kassaras et al., 2016; Haddad et al., 2020). Pick quality classes and associated errors derive from NOA (Table S2). Our preferred earthquake location software is the Non Linear Location (NLLoc) (Lomax et al., 2000) that uses a non-linear location algorithm which is thought to provide more reliable solutions and hypocentre error estimates in case of ill-conditioned locations (such as those encountered within the ZES). For more details on the earthquake relocation refer to Text S2 in the Supporting Information. Overall, the relocation of the ZES reduced the average RMS from 0.39 (revised NOA catalogue) to 0.2, with average horizontal and vertical errors of ~3.8 km (in Hypo71 format from NLLoc).

The most intriguing finding from the relocation is that, in the foreshock sequence, the vast majority of the earthquakes ruptured the upper 20 km of the crust through four main clusters (i-iv in Fig. 3a-b), each of which appears to have involved slip on multiple inferred slip surfaces (see red dashed lines in Fig. 3). Our results are broadly consistent with those of Sokos et al. (2020) and Haddad et al. (2020), although these studies focus on subsets of the ZES. Earthquake relocation highlights a prominent gap in the seismicity between Zakynthos and western

Peloponnese during the foreshock sequence, at depths ranging from ~7 to 20 km (Fig. 3a-b). This feature persists also, perhaps slightly less pronounced, during the aftershock sequence (Fig. 3c). To better evaluate possible interrelations between these clusters and assess their impact in the ZES evolution, below we constrain the kinematics of these earthquakes.

3.3 Earthquake focal mechanisms

We have obtained the moment tensors (MTs) of 102 earthquakes that occurred during the ZES by inverting regional broadband data and fitting full waveform and amplitude spectra in the time and frequency domain (Cesca et al. 2010, 2013; Heimann et al., 2018; Figs S3-S4, see the Text S3-S4 in the Supporting Information for more details). The studied earthquakes range in moment magnitude from Mw 3.9 to M_w 6.9, show shallow crustal depths down to about 25 km, and are associated with all types of faulting, with a predominance of strike-slip and thrust mechanisms (Fig. 5 and Table S4). Seventeen of these events (Figs 3 and 5) have occurred in the time-period that precedes the main earthquake (October 25th, 2018), one is the mainshock and the remaining 84 occurred during the aftershock sequence (Fig. 5).

The most interesting result of the MT inversion is that it demonstrates a high variability of MT configurations and faulting style over a quite compact region, extending laterally less than 60 km (Figs 1 and 5). Most of the 102 MT solutions could be classified (Cesca, 2020; see Fig. S5) into 8 families, each sharing similar focal mechanisms, spanning from pure strike-slip to pure thrust and normal faulting. The variability in these mechanisms is consistent with a NE-SW trending pressure axes, in agreement with the convergence direction, and a NW-SE tension axis (Fig. 5c). This faulting style complexity is supported by offshore seismic-reflection profiles (e.g., Kokkalas et al., 2013; Wardell et al., 2014; this study) that indicate abundance of deep-thrust and shallow normal faulting as well as steeply dipping strike-slip faults (Fig. 4). This is also evidenced in the diverse present-day crustal stress field inferred from regional-scale inversion of focal mechanisms (Konstantinou et al., 2017). Further, our data support a clear difference among the distribution and predominance of different focal mechanisms before and after the mainshock (Figs 3 and 5). Results suggest the activation of a complex, shallow (< 20 km) fault network and the presence of strong stress heterogeneities, probably induced or enhanced by the occurrence of the M_w 6.9 event in the ZES, which was able to trigger microseismicity across a range of fault geometries and faulting styles (Fig. 5c). The average depth of reverse faulting, which occur mostly at the western edge of the hypocentral cloud of the main event, is ~10 km, while for strike-slip and normal faulting, which occurs also east of Zakynthos and on Peloponnese, is ~8 and 9 km, respectively (Table S4 and Figs. S6-S7).

3.4 Foreshock kinematics

In the years preceding the ZES, the focal region is characterized by diffuse seismicity that highlights different local spatial clusters and different styles of faulting (Figs 3a-b, 5a). Most prominent clusters are found at about 37.5°N, 20.6°E, in the vicinity of the 2018 M_w 6.9 mainshock and close to the Peloponnese coastline, both onshore and offshore (Figs 3a-b, 5a). The clusters appear to mostly delineate along a NW-SE direction (Fig. 3a-b), marking known active faults both offshore western Peloponnese (Kokkalas et al., 2013; Wardell et al., 2014; Makris and Papoulia, 2014; Haddad et al., 2020) and onshore (Fountoulis et al., 2015), some of which have recently hosted large-magnitude historic earthquakes (e.g., the 1997 M_w 6.5 Strofades earthquake; Kiratzi and Louvari, 2003) (Fig. 1). In addition to the NW-SE striking earthquake clusters, a NE-SW cluster in onshore Peloponnese appears to delineate the large NE-SW right-lateral strike-slip Movri Fault that produced the 2008 M6.4 Movri Earthquake (Fig. 3a-b and Fig. S2a-b) (Konstantinou et al., 2009; Cesca et al. 2010). This fault is active during the ZES foreshock sequence down to depths of ~20 km (Movie S1). Indeed, distinct deep (c. 0-20 km) and shallow (< 5 km) seismicity clusters from June to November 2015 and from May to August 2016, respectively, highlight intermittent activity on sections of the Movri Fault (Movie S1 and Fig. S14). The horizontal (dextral) sense of slip on this fault is further supported by the strike-slip focal mechanisms recorded along this structure prior to the main event (Fig. 5a).

Moment tensor analysis (Fig. 5) coupled with earthquake relocation (Fig. 3) suggest that the early phase of the ZES involved slip on a series of steeply dipping NW-SE trending left-lateral strike-slip faults offshore western Peloponnese, at depths ranging from 15 to 20 km (see along-strike distance of 120-130 km on Profile A-A' in Figure 3a). The predominantly sinistral strike-slip faulting is in agreement with focal mechanisms obtained by Haddad et al. (2020). In the following 3.5 years, seismicity migrated first eastward (towards onshore Peloponnese), involving strong interactions between faults immediately offshore and onshore western Peloponnese (Fig. 3a-b) while earthquake activity west of Zakynthos was minimal, and from

November 2015 until October 2018, the seismicity of the ZES migrated westward, towards the epicentral area of the M_w 6.9 event (Movie S1). During the entire foreshock sequence (1-1-2014 to 25-10-2018), the ZES involved slip on mainly strike-slip and normal faults, with negligible contribution of thrust faulting (Fig. 3a & b, Fig. 5).

3.5 Mainshock and aftershock kinematics

The mainshock of the Zakynthos Earthquake is characterized by an oblique (thrust to strike-slip) mechanism. A full moment tensor inversion suggests a significant non-double-couple component (Fig. 6), as proposed also by global catalogues (Global CMT) and previous studies (e.g. Sokos et al. 2020). This MT solution is compatible with the combination of two sources (as proposed also by Sokos et al., 2020), one characterized by thrust faulting, similar to those resolved for a cluster of aftershocks north of the mainshock hypocenter, and one by strike-slip to oblique mechanism, as found for several aftershocks east of the mainshock hypocentre (Fig. 5b and Fig. S6). These two individual sources share a common pressure axis with our overall MT solutions (Fig. 5c and Fig. 6).

The aftershock sequence of the Zakynthos Earthquake appears outstanding in its heterogeneities. Seismicity spreads over about 60 km along the trench and 50 km across it (Figs 3c and 5b), and involves all type of earthquake types, including strike-slip, normal, thrust and oblique faulting (Fig. 5c), suggesting complex fault patterns on multiple faults of different depths and orientations. This is in agreement with local stress heterogeneities and fault diversity suggested for the study area by Konstantinou et al. (2017). The spatial distribution of the aftershocks presents two main trends: (1) the progressive localisation of aftershocks towards the epicentral area of the main event (Fig. 3c), and (2) long-range (>50 km) interactions between the epicentral region and earthquakes occurring within clusters (i) and (ii) (Fig. 3c). The latter fault interactions initiated ~2 months after the mainshock and are animated in Movie S1.

The mainshock and some aftershocks (Fig. 5b) suggest the rupture of an NNE-SSW striking and ESE-dipping (~50°) thrust fault, which most likely reflects a thrust fault in the overriding plate (as opposed to the subduction plate-interface) (Figs 3, 5 and 6; Table S4), in agreement with results from Cirella et al., (2020) and Sokos et al., (2020). The latter is supported by published seismic-reflection and bathymetric data (Figs 1 and 4, Fig. S17) that reveal numerous ~NNW-SSE trending thrusts that dip 30-50° to the northeast, beneath Zakynthos and western Peloponnese (Sachpazi et al., 2000; Kokkalas et al., 2013; Wardell et al., 2014; Makris and Papoulia, 2014; this study) and the recording of a minor tsunami (10 cm) along the western coastline of Peloponnese that suggests rupture of the sea-bed (Cirella et al., 2020). It is also supported by the low-dipping (15-17°) angle of the plate-interface beneath the epicentral area (e.g. Halpaap et al., 2018). Nevertheless, the majority of the aftershocks mark the activation of other faults (Fig. 5b). The location, depth and focal mechanisms of the latter events are incompatible with both the mainshock rupture plane and the geometries recorded during the foreshock activity (Figs. 3 and 5). Specifically, joint analysis of the location and mechanisms of the aftershock sequence suggests the activation of multiple steeply-dipping strike-slip faults that run in ~NE-SW orientations (and at high angles to the trench). The seismicity is confined above the subduction interface (<20 km) and deepens accordingly towards the coast of the Peloponnese (Fig. 5e-f). A second family of events (blue in Figs 5b-f) denote normal faulting along one or more additional NW-SE faults. Normal faulting earthquakes mostly occurred at shallow depths, indicating reactivation in the aftershock sequence of shallow normal faults located mostly on the hangingwall of thrust faults (Kokkalas et al., 2013; Wardell et al., 2014; this study) (Fig. 4). It is noteworthy that focal mechanisms between the island of Zakynthos and western Peloponnese (cluster ii in Fig. 3a-b) mark a similar region as in the years preceding the main event, but with different mechanisms (Fig. 5), suggesting that stress perturbations during the mainshock are able to inhibit strike-slip and oblique-normal mechanisms, which were dominant before October 25th 2018, and favour strike-slip and extensive pure thrust faulting. Fault slip reversed between the interseismic and postseismic periods has been also observed on crustal faults in Chile and is linked to the megathrust seismic cycle (Shirzaei et al., 2012).

4 Slow-slip events during the ZES

To assess the likely involvement of aseismic slip transients in the evolution of the ZES, we analyse the deformation on the Earth's surface recorded by 10 permanent GPS stations located within the broader study area (Fig. 1). We find that the earthquake activity within the ZES was accompanied by aseismic-slip release in the form of two slow slip events (SSEs). Below, we first discuss the analysis and modelling of the GPS data and, following, we present evidence for two prominent GPS transient signals – which are the first SSEs to be recorded in the HSS.

4.1 GPS time-series analysis and modelling

Continuous GPS data with daily recordings were obtained from 10 permanent GPS stations located along western Peloponnese and the island of Zakynthos (Fig. 1). We analysed the ITRF08 daily coordinates of 5 stations (TRIP, RLSO, PYRG, PYL1 and PAT0) available at the NEVADA Geodetic Laboratory (http://geodesy.unr.edu/magnet.php; Blewitt et al., 2018) and of 5 stations (063A, 003A, 028A, 030A, 029A) that belong to the HEPOS network of the Hellenic Cadastre. Collectively, our GPS dataset provides observations for a period of ~5.5 years (from 01.01.2014 till 31.05.2019) which is comparable to the time-period of the ZES (Fig. 2e). The recordings at stations PYRG, RLSO and TRIP have, however, slightly shorter duration (see Fig. 2d and Supplementary Figs S8-S9). For more details on the geodetic dataset used in this study see Text S5 in the Supporting Information.

As a first step in our analysis, we removed outliers from the GPS signal by applying the Hampel filter, a common approach for reducing noise (Pearson, 2005). Subsequently, we applied the Greedy Automatic Signal Decomposition algorithm (GrAtSiD; Bedford and Bevis, 2018) to decompose the GPS signal into (i) the seasonal oscillation signal; (ii) secular and transient motions and (iii) the residual signal. The secular motion corresponds to the long-term velocity of the station, which is in principle stable, while the transient signal is estimated by fitting a minimum number of multi-transient signals that are defined as the sum of two or more exponentially decaying time functions. The modelled signal is derived by using a linear regression representing a trajectory model (see Bevis & Brown, 2014). The onset of the transient signal is not pre-defined, as GrAtSiD automatically detects possible transient onsets. We applied the GrAtSiD time series decomposition using a station-by-station and component-by-component approach (Fig. S8). This process was repeated 250 times in order to retrieve the statistical information (median and interquartile range) of the 250 modelled trends (red lines in Figs S8 and S9) resulting, thus, in a time-dependent estimate of the velocity uncertainty.

Transient signals in GPS timeseries may be tectonic (e.g., Wallace and Beavan, 2010) but may also be due to environmental or anthropogenic conditions, such as high precipitation rates or monument instability (Williams et al., 2004; Larson et al., 2008). To account for non-tectonic signal, we assessed the maintenance history of all ten stations used in this analysis as well as the fluid loading history in the area. The latter was predicted at each station location based on the ESMGFZ model (http://rz-vm115.gfz-potsdam.de:8080/repository), which produces values of elastic surface loading (Dill and Dobslaw, 2013; doi:10.1002/jgrb.50353). Transient signal in the fluid loading timeseries was modeled using GrAtSiD (Fig. S11 and Movie S2). Results suggest that there is no strong correlation in space and/or time between the two GPS transients and the predicted fluid transients, which are mostly very short-lived (Fig. S11 and Movie S2). Therefore, the recorded transients are very likely tectonic.

4.2 Slip transients during the ZES

Tectonic transient signals in a GPS timeseries may be related to SSEs and/or post-seismic relaxation (e.g., Sun et al., 2014). The latter is excluded because there is no large (M>6) earthquake in the foreshock sequence (Bedford et al., 2016). To assess the spatiotemporal changes of the GPS velocity pattern within the study area, we calculate the daily median GPS network velocity along the east component, which is normal to the trench (Fig. 2e). Examination of Figure 2e reveals two significant changes in the GPS velocities both associated with an eastward acceleration of the mean velocity of the vectors before their abrupt westward rotation (Fig. 2e). The first of these transients occurs in late 2014 and lasts slightly more than 6 months, while the second starts in mid-2018 and continues until prior to the M_w 6.9 earthquake, lasting for about 5 months (Fig. 2e, Fig. 7). Here, we need to clarify that although the transient signal lasts for about 6 and 5 months during the 2014 and 2018 episodes, respectively, the slow slip events themselves have shorter duration (112 days in 2014 and 107 days in 2018; see Fig. 2e and Text S5 in the Supp. Information). This is because each transient signal comprises individual deformational periods of different durations that include, successively, landward network acceleration, trenchward network acceleration (i.e. the SSE) and, for the 2018 transient, landward network acceleration until the main M_w 6.9 event (see below for details). The daily evolution of these velocities, and the associated deformational periods within each transient, can be seen in Movie S3 whereas the interrelation between these SSEs and the seismic-moment release is highlighted in Movie S1.

The first transient initiates at 24.09.2014 and terminates at 20.03.2015 (that is, a total of 178 days) (Fig. 2e and Movie S3). During this episode all ten stations appear, first, to accelerate eastwards for about two months and, subsequently, to deviate from their main equilibrium position and rotate westwards (Figs 2e and 7a & 7c and Movie S3). Maximum cumulative displacement of about 5 mm is recorded at station 028A in Zakynthos, while attenuated displacements are observed in eastern and southern Peloponnese (e.g. stations 030A, 063A and TRIP; Fig. 7). The small vector obliquity observed at station 028A in Zakynthos with respect to vectors in Peloponnese, possibly indicates the involvement in this slow-slip event of additional (mainly strike-slip) structures of offshore Peloponnese (e.g., Bürgmann, 2018). No significant microseismicity is associated with this SSE (Movie S3).

The second transient signal spans the time-period between 14.05.2018 and 25.10.2018 (~164 days), immediately preceding the M_w 6.9 Zakynthos Earthquake (Fig. 2e). This SSE shows very similar characteristics to those recorded during the 2014-2015 transient (e.g., acceleration and trenchward rotation of the vectors; see Fig 2e, Fig 7d and Movie S3). Here, the vector acceleration lasts also for ~2 months, followed by a trenchward rotation of the vectors (Fig 2e, Fig 7 and Movie S3) and velocity acceleration until the Zakynthos mainshock (Fig. 7d). Interestingly, here, station 028A at Zakynthos Island records each deformational phase (acceleration/rotation/readjustment and acceleration) with a time delay of ~30 days compared to the remaining stations (see Movie S3). This likely suggests an upward migration of slip from greater depths (beneath Peloponnese) to shallower depths (beneath Zakynthos). Similarly to the 2014 SSE, cumulative maximum displacement is observed on Zakynthos (station 028A) and is of comparable size (5.3 mm) to the 2014 transient. This transient is associated with shallow (<10 km) seismic-moment release proximal to the epicentral area (Movie S1 and Fig. S15).

The widespread occurrence of deformation along the entire western Peloponnese and Zakynthos Island, coupled with the trenchward orientation of the vectors (Fig. 7a-b), collectively suggest that both transients likely originate on the subduction plate-interface that extends beneath central-western Peloponnese. To better explore the origin and spatial distribution of these two transients we performed forward modelling and, assuming a homogeneous elastic half-space and using the analytical equations of Okada (1985), obtained surface displacements by assigning slip on the plate-interface (Fig. S12). After testing for various displacement scenarios we derived, for each SSE, the best uniform-slip model by allowing average slip of 5 mm on the plate-interface (Fig. S12c). The total geodetic moment released during each SSE is 3.20×10^{18} Nm and corresponds to a M_w ~6.3 earthquake (Table S1). The relationship between geodetic moment release / duration of the Zakynthos transients is similar to the relationships observed for other tectonic transient signals globally (Fig. S13; Peng and Gomberg, 2010), reinforcing the tectonic origin of these deformational episodes. Some discrepancies observed in the north of the study area (Fig. S12), likely reflect additional distributed slip on the plate-interface and/or upper-plate faults. Thus, the estimated average slip of 5 mm on the plate-interface should be considered as the minimum slip required for reproducing the observed surface deformation. Slip-inversion of the transient events will allow better assessment of their spatial distribution and is currently in progress (Saltogianni et al. Pers. Com). Further, the acceleration of the vectors observed prior to both slow-slip events was recorded in all 10 stations to last for about 2 months in each case (Fig 2e, Fig. 7 and Movie S3). This acceleration may be indicative of deep active processes related to changes in slab pull force (Bedford et al., 2020) and/or to a dynamic increase of locking along the plate-interface zone prior to seismic or aseismic slip events (Materna et al., 2019). The described SSEs of this study are the first to be reported in the HSS.

5 The preparatory phase leading to the M6.9 Zakynthos Earthquake

Our data suggest that the b-values in the ZES systematically dropped below 1 soon after the trenchward rotation of the GPS velocity vectors during the 2014-2015 transient (Fig. 2d-e and Supplementary Fig. S1c). Since that time, and until the main event in late 2018, the b-values in the ZES remained overall suppressed (<1), with one exception: the ~6-months (September 2016 to April 2017) where swarm-like microseismicity ruptured repeatedly the epicentral area accounting for high b-values (up to 1.36) and strong spatiotemporal earthquake clustering (Fig. 3b, Supplementary Fig. S2c and Movie S1); note that high b-values were again encountered only in the aftershock sequence (b~1.2; Fig. 2d). Suppressed b-values (<1) have been observed prior to mainshocks globally (e.g. Nuannin et al., 2005; Schurr et al. 2014). On the other hand, elevated b-values (>1) often characterise aftershock sequences and/or earthquake swarms (Scholz, 2015; Gulia et al. 2018). The fluctuations recorded in the b-values of the ZES during the ~5 years preceding the mainshock are in accordance with these observations (Fig. 2d), with low b-values (<1) most likely indicating increased stresses in the crust during the years preceding the main event (Schorlemmer et al., 2005).

Combining the above, we propose a scenario in which the SSE that occurred beneath western Peloponnese in late 2014, tectonically destabilized (b<1) the western termination of the subduction system to, first, trigger swarm-like activity in the epicentral area of the main-shock in late 2016 and, subsequently, the M_w 6.9 Zakynthos Earthquake (Figs. 2 and 3). As discussed in Section 4.2, it is likely that the first SSE involved, in addition to slip on the plate-interface, a triggered slow-slip on one (or more) strike-slip structures in the upper-plate (see vector obliquity between Zakynthos/mainland in Fig. 7a), a scenario that could promote widespread stress changes in the upper-plate (e.g. Hamling and Wallace, 2015). The persisting low (<1) b-values in the ZES after the first SSE and until the M_w 6.9 Zakynthos Earthquake about 4.5 years later, suggests significant stress perturbations which were not fully accommodated during the swarm seismic-moment release (equivalent to a ~M_w 4.9; Table S1) in the broader epicentral area of the Zakynthos mainshock. Interestingly, following these swarms, the epicentral area remained mostly quiet for the following year (from May 2017 to April 2018; Movie S1) before it becomes next active with the onset of the second transient in May 2018 (Movie S1 and Fig. S15).

The second transient immediately precedes the main M_w 6.9 Zakynthos Earthquake (Fig 2d,e and Fig. 7b; Movie S3). The ~30 day phase-lag recorded in the reversal of the GPS vectors between Zakynthos (028A) and the rest of western Peloponnese (e.g., 030A, 029A, etc.), suggests the gradual up-dip migration of slip along the plate-interface, from ~40 km depth beneath Peloponnese to shallower crustal depths (<20 km) near Zakynthos (Fig. 7d and Movie S3). It is possible for SSEs that operate either on the subduction plate-interface (Wallace and Beavan, 2010) or nearby crustal faults (Hamling and Wallace, 2015; Bürgmann, 2018), to trigger stress changes in the crust that would lead to generation of large-magnitude earthquakes. Whether this up-dip slip migration a few days before the mainshock produced static-stress changes on one or more upper-plate faults (King et al., 1994) capable of triggering the Zakynthos Earthquake, is investigated in a follow-up study (Saltogianni et al. Pers. Com).

6 Interplay between seismic and aseismic deformation at the termination of the HSS

Our analysis records successive phases of seismic and aseismic deformation during the build-up to the M_w 6.9 Zakynthos Earthquake. One question that arises is what drives this type of deformation and how representative this may be in accommodating plate-motion over multiple earthquake–cycles. Slow-slip events that trigger swarm activity and/or moderate-to-large-sized earthquakes have been recorded before in major subduction zones globally, including New Zealand, Japan, Ecuador, Chile and Mexico (Beavan et al., 2007; Kato et al., 2012; Vallée et al., 2013; Ruiz et al., 2014; Obara and Kato, 2016; Colella et al., 2017). Although the detailed distribution of interseismic coupling beneath western Peloponnese in Greece has not been constrained, a first-order difference between the global examples and the Greek case is that the SSEs here occur on a weak plate-interface that largely creeps (Vernant et al., 2014; Saltogianni et al., 2020). The only other references for SSEs along creeping sections of the plate-interface (or sections with heterogeneous interseismic coupling) is at the central/northern Hikurangi margin in New Zealand (Wallace et al., 2016), in Ecuador (Vallee et al. 2013), Costa Rica (Davis et al. 2015) and the Boso Peninsula in Japan (Ozawa et al. 2007). In all these cases, however, the SSEs occur near the trench, at shallow (<10 km) sections of the plate-interface, and are accompanied by intense earthquake activity. By contrast, the SSEs at Zakynthos are deep (~20-40 km) and mostly seismicity free (Movie S3).

One possible explanation for the occurrence of aseismic transients at these depths of the HSS (i.e. 20-40 km) is that they mark the downdip end of locally isolated locked patches (Lay, 2015). Such patches have been recently discovered south of Crete (Saltogianni et al., 2020) and between Crete and Peloponnese (Howell et al., 2017), where they locally appear to accumulate interseismic strain that may account for up to 85% of the plate-motion. Seismic tomography coupled with analysis of seismic attributes beneath the area of ZES suggests the existence of a high (~1.9) Vp/Vs ratio zone at crustal depths ranging between ~10-30 km (Halpaap et al., 2018), which is indicative of water-rich fluids (Audet et al., 2009) (Fig. 8). As SSEs require very low effective stress (e.g., near lithostatic pore fluid pressures) and high fluid pressures (e.g., Liu and Rice, 2005; Gao and Wang, 2017), their presence beneath western Peloponnese is not surprising. Further, studies have shown that fluids liberated from the plate-interface during SSEs tend to migrate upwards, into the lower portion of the seismogenic zone (Audet et al., 2009; Nakajima and Uchida, 2018) to trigger widespread microseismicity, often in the form of earthquake swarms. The network of strike-slip faults onshore/offshore western Peloponnese (Figs. 1 and 4) is likely to have acted as conduits for fluid migration and triggering of microseismicity within the ZES (Fig. 8), as it is the case with upper-plate faults elsewhere in the Hellenic forearc (Ruscic et al., 2019).

Recurring slow-slip events are common along subduction margins and in some cases (e.g., Nankai Trough megathrust) they appear to accommodate up to >50% of the total plate-motion (Araki et al., 2017). In Greece, two SSEs and significant microseismicity are recorded over a period of ~5 years to precede a large event (Fig. 2d). A question that arises is what percentage of the plate-motion is accommodated by each process operating at the western-end of the HSS. To address this question we have quantified the contribution of each component of deformation (seismic and aseismic) for the period that precedes the M_w 6.9 event (Table S6; for details refer to Text S6 of Supplementary Information). We find that the aseismic slip-rate (produced collectively by the two SSEs) amounts to ~2.1 mm/yr (or ~8% of the plate-motion), accommodating significantly more subduction-related strain compared to that produced by the ZES seismicity (slip-rate ~1.3 mm/yr or 5% of the plate-motion) (Table S6). These numbers collectively imply that during the ~5 years preceding the Zakynthos Earthquake, at least 15% of the plate-motion was released, ~70% was stored elastically (on upper-plate faults and/or the plate-interface), while the remaining ~15% was accommodated by aseismic creep along the downgoing plate (Table S6). Knowing that the average locking along the Hellenic subduction interface is weak (Vernant et al., 2014; Saltogianni et al., 2020) and that the crust beneath the ZES is broken up by numerous upper-plate faults (Figs 1, 4 and 8), we anticipate that a significant fraction of the 70% interseismic strain was stored on one or more faults in the overriding plate. That was confirmed by the M_w 6.9 Zakynthos Earthquake that followed and ruptured faults in the upper crust (Fig. 8). Further, analysis of the aftershock sequence shows that, during the six months following the mainshock, strain equivalent to ~75% of the plate-motion was accommodated by upper-plate faults (Table S1). Similar kinematics characterise the southern termination of the Hikurangi margin in New Zealand, where about 80% of the plate-motion (Wallace et al., 2012) and seismic-moment release during large-magnitude earthquakes (Mouslopoulou et al., 2019) are accommodated by upper-plate faults. Composite faulting patterns accompanied by alternating styles of deformation may characterise multi-fault subduction-termination zones. Our data support the view that the aseismic and seismic displacements observed within the ZES ~5 years prior to the M_w 6.9 Zakynthos Earthquake are probably manifestations of very late interseismic stress conditions (i.e. Schurr et al., 2014). Whether these features characterise the seismogenesis at the western termination of the HSS will be tested as additional data from future well-monitored large-magnitude earthquakes become available.

7 Conclusions

We have studied the deformation of the Earth's crust where active subduction zones terminate prior and after the 2018 M_w 6.9 Zakynthos Earthquake. Using earthquake, GPS, seismic-reflection and bathymetric data we find that the mainshock was preceded by a synergy of slow-slip events, earthquake swarms and fault-interactions between the subduction thrust and upper-plate faults that lasted about 5.5 years. This long-lasting preparatory phase initiated due to a plate-interface slow-slip event that released strain equivalent to a ~M_w 6.3 earthquake, tectonically destabilising the upper 20-40 km of the crust and producing alternating phases of seismic and aseismic deformation between the upper-plate and the plate-interface. Tectonic deformation included intense microseismicity (M<4) on neighbouring faults, earthquake swarms in the epicentral area of the mainshock, another episode of slow-slip immediately preceding the mainshock and, eventually, the large (M_w 6.9) Zakynthos Earthquake. Tectonic instability in the area is evidenced by a prolonged (~3.5 years) period of overall supressed b-values (<1) and strong earthquake interactions on discrete strike-slip, thrust and normal faults. Composite faulting patterns accompanied by alternating (seismic/aseismic) deformation styles may reflect late interseismic stress conditions prior to large-magnitude earthquakes that rupture subduction-termination zones.

Acknowledgments

We thank the staff of the Institute of Geodynamics of the National Observatory of Athens and all partners of the HUSN (including the University of Patras, the University of Thessaloniki, and the University of Athens), for data archiving/processing. In this analysis we used seismological data from stations pertaining to the following networks: GE, IU, II, G, MN, IV, HT, HP, HA, AC, 4A, X5 (data link : http://www.gein.noa.gr/en/networks/husn); seismic data and metadata have been downloaded using the FDSN web services of Orfeus (https://www.orfeus-eu.org/data/eida/webservices/dataselect/), INGV (https://doi.org/10.13127/SD/X0FXNH7QFY), NOA (https://doi.org/10.7914/SN/HL), IRIS (https://service.iris.edu/fdsnws/) and Geofon (https://doi.org/10.14470/TR560404). We are also grateful to the Greek Cadastre (063A, 003A, 028A, 030A, 029A) and NEVADA Geodetic Laboratory (i.e., TRIP, RLSO, PYRG, PYL1 and PAT0) for providing the GPS timeseries of the corresponding permanent stations. Many thanks to Dr Dirk Becker for useful discussion on the b-value calculation and to Dr John Begg for help with the block-diagram drawing in Figure 7.

References

Aki, K. (1966). Generation and Propagation of G Waves from the Niigata Earthquake of June 16, 1964: Part 2. Estimation of earthquake moment, released energy, and stress-strain drop from the G wave spectrum. *Bulletin of the Earthquake Research Institute, University of Tokyo*, *44*, 73-88.

Albuquerque Seismological Laboratory (ASL)/USGS (1988). Global Seismograph Network - IRIS/USGS. International Federation of Digital Seismograph Networks. Dataset/Seismic Network. 10.7914/SN/IU.

Anderson, H., & Jackson, J. (1987). Active tectonics of the Adriatic region. *Geophysical Journal of the Royal Astronomical Society,* 91, 937-983.

Araki, E., Saffer, D., Kopf, A., Wallace, L., Kimura, T., Machida, Y., Ide, S., Davis, E., & IODP Expedition 365 Shipboard Scientists (2017). Recurring and triggered slow-slip events near the trench at the Nankai Trough subduction megathrust. *Science,* 356, 1,157–1,160, https://doi.org/10.1126/science.aan3120.

Audet, P., Bostock, M.G., Christensen, N.I., & Peacock, S.M. (2009). Seismic evidence for overpressured subducted oceanic crust and megathrust fault sealing. *Nature,* 457, 76–78. http://dx.doi.org/10.1038/nature07650.

AUTH (Aristotle University of Thessaloniki) (1981). Aristotle University of Thessaloniki Seismological Network. International Federation of Digital Seismograph Networks. 10.7914/SN/HT, https://doi.org/10.7914/SN/HT.

Beavan, J., Wallace, L., Douglas, A., & Fletcher, H. (2007). Slow slip events on the Hikurangi subduction interface, New Zealand, in Dynamic Planet: Monitoring and Understanding a Dynamic Planet With Geodetic and Oceanographic Tools: IAG Symposium, Cairns, Australia, 22–26August, 2005, Int. Assoc. Geod. Symp., 130, edited by P. Tregoning and C. Rizos, 438–444, Springer, Berlin.

Bedford, J., Moreno, M., Li, S., Oncken, O., Baez, J.C., Bevis, M., Heidbach, O. & Lange, D. (2016). Seperating rapid relocking, afterslip, and viscoelastic relaxation: An application of the postseismic straightening method to the Maule 2010 cGPS. *Journal of Geophysical Research,* 121, 7618—7638.

Bedford, J., & Bevis, M. (2018). Greedy automatic signal decomposition and its application to daily GPS time series. *Journal of Geophysical Research*, 123, B014765, 6992–7003.

Bedford, J., Moreno, M., Deng, Z., Oncken, O., Schurr, B., John, T., Báez, J.C., & Bevis. M. (2020). Months-long thousand-km-scale wobbling before great subduction earthquakes, *Nature*, 580, 628-635.

Bevis, M., & Brown, A. (2014). Trajectory models and reference frames for crustal motion geodesy. *Journal of Geodesy*, 88, 283-311.

Blewitt, G., Hammond, W.C., & Kreemer, C. (2018). Harnessing the GPS data explosion for interdisciplinary science. Eos 99, https://doi.org/10.1029/2018EO104623.

Bouchon, M., Durand, V., Marsan, D., Karabulut, H.. & Schmittbuhl, J. (2013). The long precursory phase of most large interplate earthquakes. *Nature Geoscience*, 6, 299–302, *doi*:*10.1038/ngeo1770*.

Bürgmann R. (2018). The geophysics, geology, and mechanics of slow fault slip. *Earth and Planetary Science Letters*, 495, 112–34.

Cesca, S., Heimann, S., Stammler, K., & Dahm, T. (2010). Automated procedure for point and kinematic source inversion at regional distances. *Journal of Geophysical Research*, 115, doi:10.1029/2009JB006450

Cesca, S., Rohr, A., & Dahm, T. (2013). Discrimination of induced seismicity by full moment tensor inversion and decomposition. *Journal of Seismology*, 17, 1, 147-163, doi:10.1007/s10950-012-9305-8.

Cesca, S., Zhang, Y., Mouslopoulou, V., Wang, R., Saul, J., Savage, M., & et al. (2017). Complex rupture process of the Mw 7.8, 2016, Kaikoura earthquake, New Zealand, and its aftershock sequence. *Earth and Planetary Science Letters*, 478, 110-120.

Cesca, S. (2020). Seiscloud, a tool for density-based seismicity clustering and visualization. *Journal of Seismology*, https://doi.org/10.1007/s10950-020-09921-8

Cirella, A., Romano, F., Avallone, A., Piatanesi, A., Briole, P., Ganas, A. & et al. (2020). The 2018 M w 6.8 Zakynthos (Ionian Sea, Greece) earthquake: seismic source and local tsunami characterization. *Geophysical Journal International*, 221, 1043-1054.

Clément, C., Hirn, A., Charvis, P., Sachpazi, M., & Marnelis, F. (2000). Seismic structure and the active Hellenic subduction in the Ionian islands. *Tectonophysics*, 329, 141–156.

Colella, H.V., Sit, S.M., Brudzinski, M.R., Graham, S.E., Demets, C., Holtkamp, S.G., & et al. (2017). Seismicity rate increases associated with slow slip episodes prior to the 2012 Mw 7.4 Ometepec earthquake. *Earth and Planetary Science Letters*, 464, 35–45.

Davis, E.E., Villinger, H., & Sun T. (2015). Slow and delayed deformation and uplift of the outermost subduction prism following ETS and seismogenic slip events beneath Nicoya Peninsula, Costa Rica. *Earth and Planetary Science Letters,* 410, 117–27.

Dziewonski, A.M., Chou, T.-A., & Woodhouse, J.H. (1981). Determination of earthquake source parameters from waveform data for studies of global and regional seismicity. *Journal of Geophysical Research,* 86, 2825-2852, doi:10.1029/JB086iB04p02825

Ekström, G., Nettles, M., & Dziewonski, A.M. (2012). The global CMT project 2004-2010: Centroid-moment tensors for 13,017 earthquakes. *Physics of the Earth Planetary Interior,* 200-201, 1-9, doi:10.1016/j.pepi.2012.04.002.

Fountoulis, I., Vassilakis, E., Mavroulis, S., Alexopoulos, J., Dilalos, S., & Erkeki, A. (2015). Synergy of tectonic geomorphology, applied geophysics and remote sensing techniques reveal the existence of active tectonism in NW Peloponnese (Greece). *Geomorphology,* 237, 52-64.

Gao, X., & Wang, K. (2017). Rheological separation of the megathrust seismogenic zone and episodic tremor and slip. *Nature*, 543, 416-419.

GEOFON Data Centre, 1993. *GEOFON Seismic Network*. Deutsches GeoForschungsZentrum GFZ. https://doi.org/10.14470/TR560404

Grigoli, F., Cesca, S., Rinaldi, A.P., Manconi, A., Lopez Comino, J.A., Clinton, J.F., et al. (2018). The November 2017 Mw 5.5 Pohang earthquake: A possible case of induced seismicity in South Korea, *Science*, 360, 6392, 1003-1006, doi:10.1126/science.aat2010.

Gulia, L., Rinaldi, A. P., Tormann, T., Vannucci, G., Enescu, B., & Wiemer, S. (2018). The effect of a mainshock on the size distribution of the aftershocks. *Geophysical Research Letters,*45, 13-277.

Haddad, A., Ganas, A., Kassaras, I., & Lupi, M. (2020). Seismicity and geodynamics of western Peloponnese and central Ionian Islands: insights from a local seismic deployment, *Tectonophysics*, https://doi.org/10.1016/j.tecto.2020.228353.

Halpaap, F., Rondenay, S., & Ottemöller, L. (2018). Seismicity, Deformation, and Metamorphism in the Western Hellenic Subduction Zone: New Constraints From Tomography. *Journal of Geophysical Research,* 123, 3000-3026.

Halpaap, F., Rondenay, S., Perrin, A., Goes, S., Ottemöller, L., Austrheim, H.O., & et al. (2019). Earthquakes track subduction fluids from slab source to mantle wedge sink. *Science Advances,* 5, doi: 10.1126/sciadv.aav7369.

Hamling, I.J., & Wallace, L.M. (2015). Silent triggering: aseismic crustal faulting induced by a subduction slow slip event. *Earth and Planetary Science Letters,* 421, 13-19; doi: 10.1016/j.epsl.2015.03.046

Hanks, T.C. & Kanamori, H. (1979). A moment magnitude scale. *Journal of Geophysical Research,* 84, 2348-2350.

Heimann, S., Isken, M., Kühn, D., Sudhaus, H., Steinberg, A., Vasyura-Bathke, H., & et al. (2018). Grond - A probabilistic earthquake source inversion framework. V. 1.0. GFZ Data Services. https://doi.org/10.5880/GFZ.2.1.2018.003

Howell, A., Palamartchouk, K., Papanikolaou, X., Paradissis, D., Raptakis, C., Copley, A., & et al. (2017). The 2008 Methoni earthquake sequence: the relationship between the earthquake cycle on the subduction interface and coastal uplift in SW Greece. *Geophysical Journal International*, 208(3), 1592–1610, doi: 10.1093/gji/ggw462

INGV Seismological Data Centre (2006). *Rete Sismica Nazionale (RSN)*. Istituto Nazionale di Geofisica e Vulcanologia (INGV), Italy. https://doi.org/10.13127/SD/X0FXNH7QFY

INGV (Istituto Nazionale di Geofisica e Vulcanologia) (2009). Emersito Seismic Network for Site Effect Studies in L'Aquila town (Central Italy). International Federation of Digital Seismograph Networks. Dataset/Seismic Network. 10.7914/SN/4A_2009

Institute of Geosciences, Energy, Water and Environment (2002). Albanian Seismological Network. International Federation of Digital Seismograph Networks. Dataset/Seismic Network. 10.7914/SN/AC

Institut De Physique Du Globe De Paris (IPGP), & Ecole Et Observatoire Des Sciences De La Terre De Strasbourg (EOST) (1982). *GEOSCOPE, French Global Network of broad band seismic stations*. Institut de Physique du Globe de Paris (IPGP). https://doi.org/10.18715/GEOSCOPE.G

Karastathis, V.K., Mouzakiotis, E., Ganas, A., & Papadopoulos, G.A. (2015). High-precision relocation of seismic sequences above a dipping Moho: the case of the January-February 2014 seismic sequence on Cephalonia island (Greece). *Solid Earth, 6*, 173-184.

Kassaras, I., Kapetanidis, V., & Karakonstantis, A. (2016). On the spatial distribution of seismicity and the 3D tectonic stress field in western Greece. *Physics and Chemistry of the Earth,* 95, 50-72.

Kato, A., Obara, K., Igarashi, T., Tsuruako, H., Nakagawa, S., & Hirata N. (2012). Propagation of slow slip leading up to the 2011 Mw 9.0 Tohoku-Oki earthquake. *Science,* 335, 705–708.

King, G.C., Stein, R.S., & Lin, J. (1994). *Static stress changes and the triggering of earthquakes. Bulletin of the Seismologial Society of America, 84, 935–953.*

Kiratzi, A., & Louvari, E. (2003). Focal mechanisms of shallow earthquakes in the Aegean Sea and the surrounding lands determined by waveform modelling: a new database. *Journal of Geodynamics,* 36, 251-274.

Kokinou, E., Kamberis, E., Vafidis, A., Monopolis, D., Ananiadis, G., & Zelilidis, A. (2005). Deep seismic reflection data from offshore western Greece: A new crustal model for the Ionian Sea*. Journal of Petroleum Geology,* 28, 185-202.

Konstantinou, K. I., Melis, N.S., Lee, S.J., Evangelidis, C.P., & Boukouras, K. (2009). Rupture process and aftershocks relocation of the 8 June 2008 Mw 6.4 earthquake in northwest Peloponnese, western Greece. *Bulletin of the Seismologial Society of America*, 99, 3374–3389, doi: 10.1785/0120080301.

Konstantinou, K. I., Mouslopoulou, V., Liang,W.-T., Heidbach, O., Oncken, O., & Suppe, J. (2017). Present-day crustal stress field in Greece inferred from regional-scale damped inversion of earthquake focal mechanisms. *Journal of Geophysical Research*, 122, 506–523. https://doi.org/10.1002/2016JB013272.

Larson, K.M., Small, E.E., Gutmann, E.D., & Bilich, A.L. (2008). Use of GPS receivers as a soil moisture network for water cycle studies. *Geophysical Research Letters,* 35, 851–854.

Lay, T. (2015). The surge of great earthquakes from 2004 to 2014, *Earth and Planetary Science Letters*, 409, 133–146.

Liu, Y., & Rice, J.R. (2005). Aseismic slip transients emerge spontaneously in three dimensional rate and state modeling of subduction earthquake sequences. *Journal of Geophysical Research,* 110, B08307, doi:10.1029/2004JB003424.

Lomax, A., Virieux, J., Volant, P., & Berge-Thierry, C. (2000). Probabilistic earthquake location in 3D and layered models, in: Thurber, C.H., Rabinowitz, N. (Eds.), *Advances in Seismic Event Location,* Springer, Dordrecht, Kluwer, Amsterdam, pp. 101–134.

Lomax, A., Michelini, A., & Curtis, A. (2009). Earthquake Location, Direct, Global-Search Methods, in: Meyers, R.A. (Ed.), Encyclopedia of Complexity and Systems Science. Springer New York, New York, NY, pp. 2449–2473.

Makris J, & Papoulia J., (2014). The backstop between the Mediterranean Ridge and western Peloponnese, Greece: its crust and tectonization. An active seismic experiment with ocean bottom seismographs. *Bollettino di Geofisica Teorica e Applicata*, 55, 249–279. https://doi.org/10.4430/bgta0125

Mann, P., & Frohlich, C. (1999). Classification and tectonic comparison of subduction to strike-slip transitions on active plate boundaries. In: Penrose Conference on Subduction to Strike-Slip Transitions on Plate Boundaries. *Geological Society of America,* Puerto Plata, Dominican Republic.

McClusky, S., Balassanian, S., Barka, A., Demir, C., Ergintav, S., Georgiev, I., et al. (2000). Global Positioning System constraints on plate kinematics and dynamics in the eastern Mediterranean and Caucasus. *Journal of Geophysical Research*, 105(B3), 5695–5719. https://doi. org/10.1029/1999JB900351

MedNet Project Partner Institutions (1990). *Mediterranean Very Broadband Seismographic Network (MedNet)*. Istituto Nazionale di Geofisica e Vulcanologia (INGV). https://doi.org/10.13127/SD/FBBBTDTD6Q

Mouslopoulou, V., Saltogianni, V., Nicol, A., Oncken, O., Begg, J., Babeyko, A., & et al. (2019). Breaking a subduction-termination from top-to-bottom: the 2016 Kaikōura earthquake, New Zealand. *Earth and Planetary Science Letters,* 506, 221-230, https://doi.org/10.1016/j.epsl.2018.10.020.

Mouslopoulou, V., & Hristopulos, D.T. (2011). Patterns of tectonic fault interactions captured through variogram analyses of microearthquakes. *Journal of Geophysical Research,* 116, B07305, https://agupubs.onlinelibrary.wiley.com/doi/pdf/10.1029/2010JB007804

Nakajima, J., & Uchida, N. (2018). Repeated drainage from megathrusts during episodic slow slip. *Nature Geoscience*, 11, 351-356

Negi, S. S., Paul, A., Cesca, S., Kamal, Kriegerowski, M., Mahesh, P., & Gupta, S. (2017). Crustal velocity structure and earthquake processes of Garhwal-Kumaun Himalaya: Constraints from regional waveform inversion and array beam modeling. *Tectonophysics,* 712, 45-63, doi:10.1016/j.tecto.2017.05.007

NOA (National Observatory of Athens), Institute of Geodynamics, Athens (1997). National Observatory of Athens Seismic Network. International Federation of Digital Seismograph Networks. Dataset/Seismic Network. 10.7914/SN/HL, https://doi.org/10.7914/SN/HL.

Nuannin P., Kulhánek, O., & Persson, L. (2005). Spatial and temporal b-value anomalies preceding the devastating off coast of NW Sumatra earthquake of December 26, 2004, *Geophysical Research Letters,* 32, L11307, doi: 0.1029/2005GL022679.

Obara, K., & Kato, A. (2016). Connecting slow earthquakes to huge earthquakes. *Science*, 353, 253-257.

Okada, Y. (1985). Surface deformation due shear and tensile faults in a half-space. *Bulletin of the Seismological Society of America,* 75, 1135–1154.

Papazachos, B., & Papazachou, C. (2003). The Earthquakes of Greece. Ziti Publication (In Greek).

Pearce, D., Rondenay, S., Sachpazi, M., Charalampakis, M., & Royden, L.H. (2012). Seismic investigation of the transition from continental to oceanic subduction along the western Hellenic subduction Zone. *Journal of Geophysical Research,* 117, 1–18. https://doi.org/10.1029/2011JB009023

Pearson K.R. (2005). Mining Imperfect Data: Dealing with Contamination and Incomplete Records, SIAM, 312 pp.

Pérouse, E., Sébrier, M., Braucher, R., Chamot-Rooke, N., Bourlès, D., Briole, P., & et al. (2017). Transition from collision to subduction in Western Greece: the Katouna–Stamna active fault system and regional kinematics. *International Journal of Earth Sciences*, 106, 967–989, doi:10.1007/s00531-016-1345-9.

Royden, L.H. & Papanikolaou, D.J. (2011). Slab segmentation and late Cenozoic disruption of the Hellenic arc. *Geochemistry, Geophysics, Geosystems*, 12, doi.org/10.1029/2010GC003280.

Ruiz, S., Metois, M., Fuenzalida, A., Ruiz, J., Leyton, F., Grandin, R., & et al. (2014). Intense foreshocks and a slow slip event preceded the 2014 Iquique *M*w8.1 earthquake. *Science*, 345, 165–1169. http://dx.doi.org/10.1126/science1256074.

Ruscic, M., Bocchini, G. M., Becker, D., Meier, T., van Keken, P.E. (2019). Variable spatio-temporal clustering of microseismicity in the Hellenic Subduction Zone as possible indicator for fluid migration. *Lithos*, *346*, 105154.

Sachpazi, M., Hirn, A., Clément, C., Haslinger, F., Laigle, M., Kissling, E., & et al. (2000). Western Hellenic subduction and Cephalonia Transform: Local earthquakes and plate transport and strain. *Tectonophysics*, 319, 301–319.

Saltogianni, V., Mouslopoulou, V., Oncken, O., Nicol, A., Gianniou, M., & Mertikas, S. (2020). Elastic fault interactions and earthquake-rupture along the southern Hellenic subduction plate-interface zone in Greece. *Geophysical Research Letters*, doi: 10.1029/2019GL086604.

Scholz, C.H. (2015). On the stress dependence of the earthquake *b*value. *Geophysical Research Letters*, 42, 1399–1402.

Schurr, B., Asch, G., Hainzl, S., Bedford, J., Hoechner, A., Palo, M., & et al. (2014). Gradual unlocking of plate boundary controlled initiation of the 2014 Iquique earthquake. *Nature*, 512, 299-302.

Scripps Institution of Oceanography (1986). Global Seismograph Network - IRIS/IDA. International Federation of Digital Seismograph Networks. Dataset/Seismic Network. 10.7914/SN/II

Shirzaei, M., Burgmann, R., Oncken, O., Walter, T.R., Victor, P., & Ewiak, O. (2012). Response of forearc crustal faults to the megathrust earthquake cycle: InSAR evidence from Mejillones Peninsula, Northern Chile. *Earth and Planetary Science Letters,* 333-334, 157-164.

Sokos, E., Gallovič, F., Evangelidis, C.P., Serpetsidaki, A., Plicka, V., Kostelecký, J., & et al (2020). The 2018 Mw 6.8 Zakynthos, Greece, Earthquake: Dominant Strike-Slip Faulting near Subducting Slab. *Seismological Research Letters*, 91, 721–732, doi: 10.1785/0220190169.

Sokos, E. (2015). Lefkada temporary network. International Federation of Digital Seismograph Networks. Dataset/Seismic Network. 10.7914/SN/X5_2015

Storchak, D.A., Di Giacomo, D., Bondár, I., Engdahl, E.R., Harris, J., Lee, W.H., & et al. (2013). Public release of the ISC–GEM global instrumental earthquake catalogue (1900–2009). *Seismological Research Letters*, 84, 810-815.

Sun, T. et al., 2014. Prevalence of viscoelastic relaxation after the 2011 Tohoku-oki earthquake. *Nature* 514, 84–87.

UA (University of Athens), (2008). Hellenic Seismological Network, University of Athens, Seismological Laboratory. International Federation of Digital Seismograph Networks. Dataset/Seismic Network. 10.7914/SN/HA

Uchida, N., Iinuma, T., Nadeau, R. M. Bürgmann, R. & Hino, R. (2016). Periodic slow slip triggers megathrust zone earthquakes in northeastern Japan. *Science,* 351, 488–492.

UP (University of Patras), 2000. University of Patras, Seismological Laboratory. International Federation of Digital Seismograph Networks. Dataset/Seismic Network. 10.7914/SN/HP

Utsu T. (1965). A method for determining the value of b in a formula 329 log n = a - bM showing the magnitude-frequency relation for 330 earthquakes. *Geophysical Bulletin, Hokkaido University*, 13, 99–103.

Vallee, M., Nocquet, J.M., Battaglia, J., Font, Y., Segovia, M., Régnier, M., & et al. (2013). Intense interface seismicity triggered by a shallow slow slip event in the Central Ecuador subduction zone. *Journal of Geophysical Research,* 118, 2965–81.

Vernant, P., Reilinger, R., & McClusky, S. (2014). Geodetic evidence for low coupling on the Hellenic subduction plate interface. *Earth and Planetary Science Letters,* 385, 122–129. https://doi.org/10.1016/j.epsl.2013.10.018

Wallace, L.M., & Beavan, J. (2010). Diverse slow slip behavior at the Hikurangi subduction margin, New Zealand. *Journal of Geophysical Research,* 115, B12402. http://dx.doi.org/10.1029/2010JB007717.

Wallace, L.M., Barnes, P., Beavan, J., Van Dissen, R., Litchfield, N., Mountjoy, J., & et al. (2012). The kinematics of a transition from subduction to strike-slip: an example from the central New Zealand plate-boundary. *Journal of Geophysical Research*, 117, B02405.

Wallace, L.M.,, Webb, S.C., Ito, Y., Mochizuki, K., Hino, R., et al. (2016). Slow slip near the trench at the Hikurangi subduction zone. *Science,* 352, 701–4.

Waldhauser, F., & Ellsworth, W.L. (2002). Fault structure and mechanics of the Hayward Fault, California, from double-difference earthquake locations. *Journal of Geophysical Research,* DOI: 10.1029/2000JB000084

Wardell, N., Camera, L., Mascle, J., Nicolich, R., Marchi, M., & Barison, E. (2014). The structural framework of the Peloponnese continental margin from Zakynthos to Pylos from seismic reflection and morpho-bathymetric data. *Bollettino di Geofisica Teorica e Applicata,* 55, 343-367.

Wiemer, S., & Wyss, M. (2000). Minimum magnitude of completeness in earthquake catalogs: Examples from Alaska, the Western United States, and Japan. *Bulletin of the Seismological Society of America*, 90, 859–869.

Williams, S.D.P., Bock, Y., Fang, P., Jamason, P., Nikolaidis, R.M., Prawirodirdjo, L. et al., (2004). Error analysis of continuous GPS position time series. *Journal of Geophysical Research*, 109, 1–19.

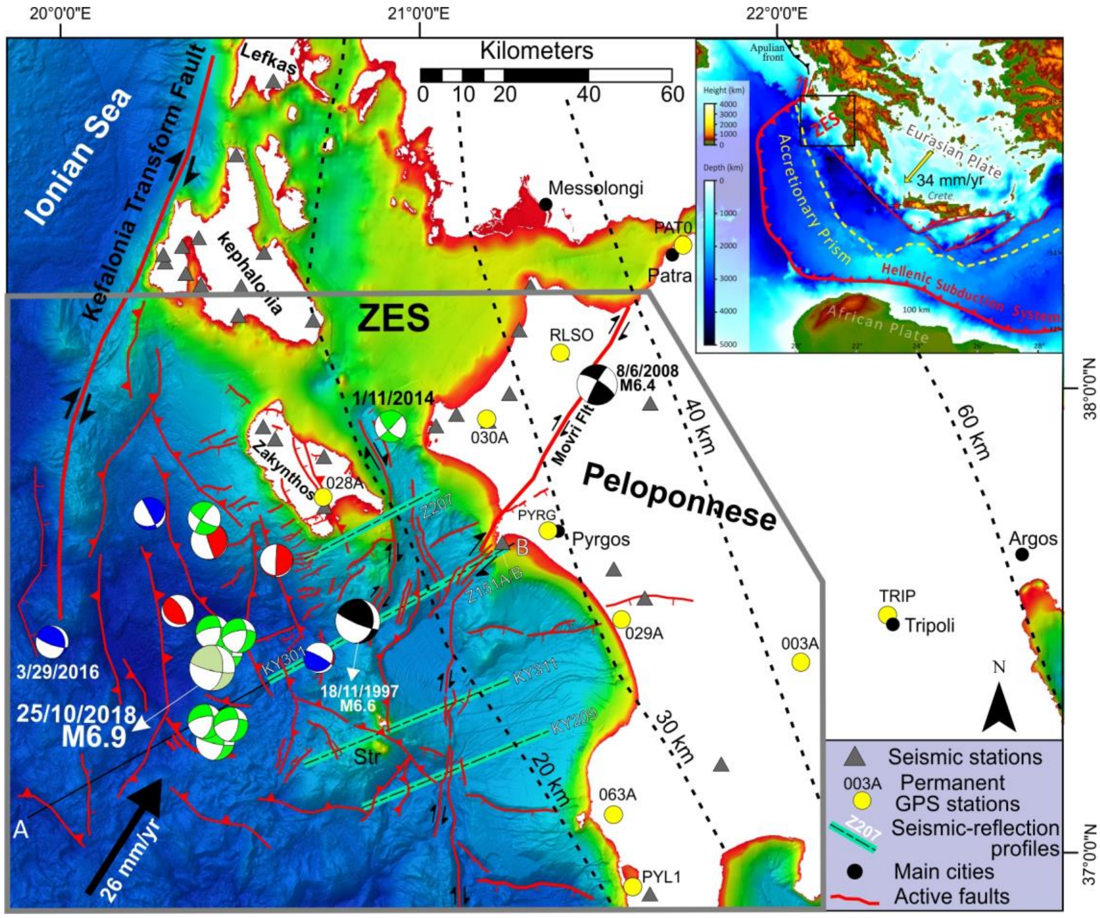

Figure 1. **Overview of the kinematics of the study area and the datasets used.** Map illustrating the major active faults in the offshore study area and the focal mechanisms of all 14 M_w>5 earthquakes that occurred during the Zakynthos Earthquake Sequence (ZES), including the M_w 6.9 main event on October 25th 2018, colour coded according to fault style (green=strike-slip, blue=normal, red=thrust). Two of these events (indicated) occurred prior to the main-shock. The black moment tensor solutions indicate the epicentres (ISC-GEM; Storchak et al., 2013) and mechanisms (Global GMT; Dziewonski et al., 1981; Ekström et al., 2012) of the two M>6 earthquakes that occurred in the study area during the instrumental period: the 2008 M6.4 Movri Earthquake onshore Peloponnese and the 1997 M6.6 Strofades Earthquake. Grey triangles indicate the seismic stations used for earthquake-relocation and calculation of moment tensor solutions, while yellow-circles localities of permanent GPS stations. Lines Z207, KY301-Z151AB, KY311 and KY209 indicate the localities of the seismic-reflection profiles from Wardell et al., 2014 (re-interpreted in Figure 4). The bathymetric profile A-B is presented in Supplementary Fig. S17. Main cities are indicated by black circles. Contours mark the top of the plate-interface (Halpaap et al., 2019). Offshore bathymetry derived from EMODnet (https://portal.emodnet-bathymetry.eu/?menu=19). Black arrow indicates the relative Eurasia-Africa plate motion (Pérouse et al., 2017). Inset: the study area is located at the western termination of the Hellenic subduction margin, the main tectonic features of which are indicated by red lines. The northward extent of the accretionary prism is indicated by yellow-dashed line. Bathymetry is from GEBCO. Stars indicate the epicentres of the 365AD (west) and 1303AD (east) earthquakes in offshore Crete. Yellow arrow indicates the relative Eurasia-Africa plate motion as derived from GPS measurements (Saltogianni et al., 2020). Str=Strofades islets.

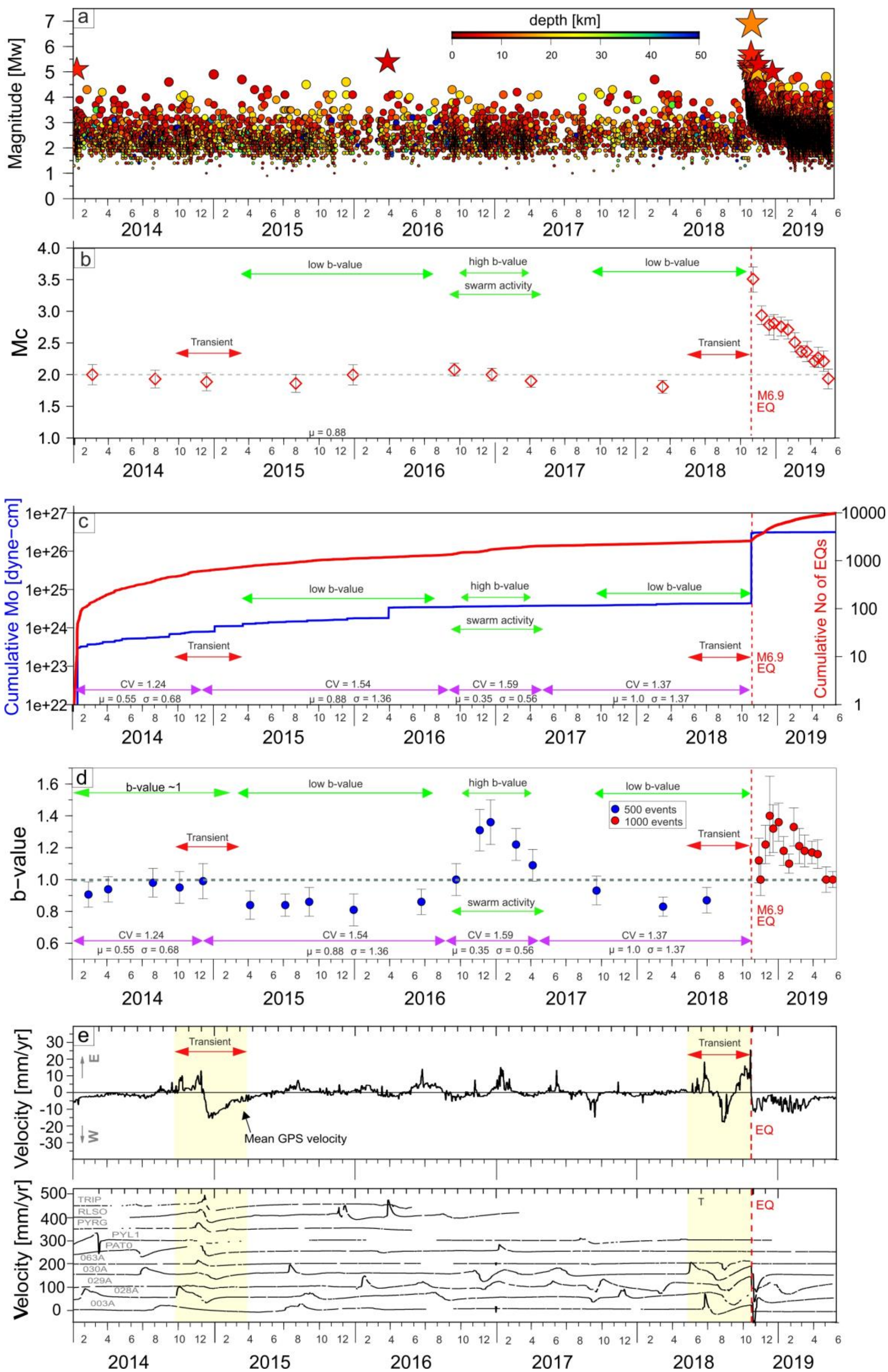
a
Magnitude [Mw]
depth [km]
b
Mc
low b-value
high b-value
swarm activity
Transient
M6.9
EQ
μ = 0.88
c
Cumulative Mo [dyne-cm]
Cumulative No of EQs
CV = 1.24
μ = 0.55 σ = 0.68
CV = 1.54
μ = 0.88 σ = 1.36
CV = 1.59
μ = 0.35 σ = 0.56
CV = 1.37
μ = 1.0 σ = 1.37
d
b-value
b-value ~1
500 events
1000 events
e
Velocity [mm/yr]
Mean GPS velocity
EQ
TRIP
RLSO
PYRG
PYL1
PAT0
063A
030A
029A
028A
003A
T
2014
2015
2016
2017
2018
2019

883

Figure 2 (previous page). **Main characteristics of the seismic and GPS deformation recorded during the ZES. a,** Moment magnitude (M_w) evolution during the Zakynthos Earthquake Sequence (ZES). Stars indicate events M>5. **b,** Evolution of magnitude of completeness (M_c)through time. **c,** Cumulative seismic-moment and cumulative number of earthquakes during the ZES as a function of time (Jan 1st, 2014 till May 31st 2019). **d,** b-value evolution (and its standard deviation) through time. High and low b-values, slow-slip events and earthquake swarms are indicated on all graphs for comparison. The coefficient of variation (CV) for each time interval is annotated. The average inter-event time (days) and the standard deviation are indicated with μ and σ, respectively. **e,** Evolution of the east GPS component during the ZES, averaged over the stations indicated in the lower panel. Trenchward motion is west. The duration of the two transients observed in the ZES is indicated by red arrows.

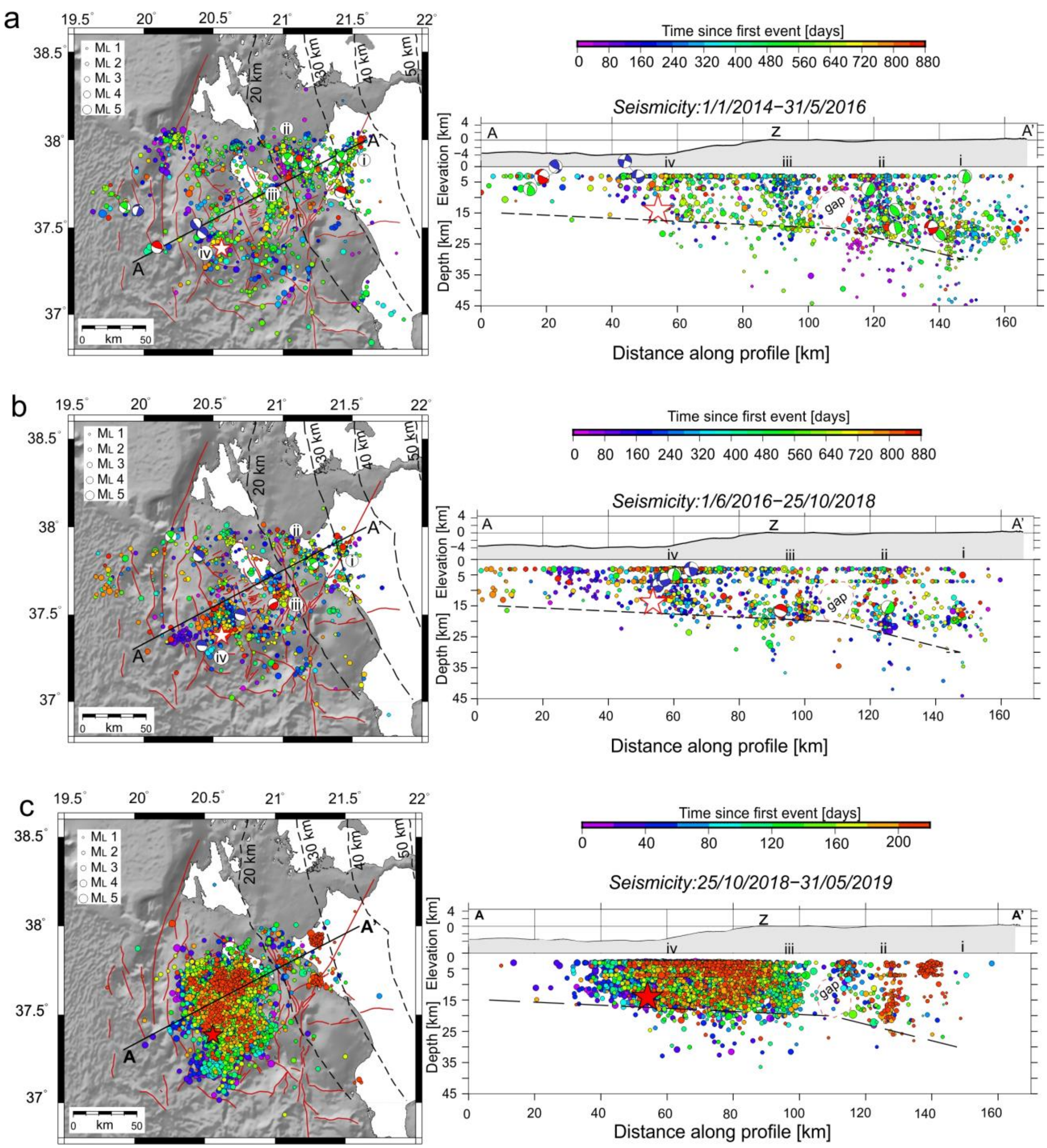

Figure 3. Spatial and temporal distribution of the ZES. Map-view and cross-section of the relocated ZES over three distinct time-intervals: **a,** January 1st, 2014 to May 31st, 2016; **b,** June 1st, 2016 to October 25th, 2018; **c,** October 25th, 2018 to May 30th, 2019. Earthquake activity in each panel is projected along the profile A-A' (70 km either side of the profile) and colour-coded according to time (see legend). Seismic events have horizontal and vertical locations errors <5 km and RMS <0.5 sec. Black dashed-lines in map-view and cross-section indicate the depth-to-the-top of the plate-interface (from Halpaap et al., 2019) while red star indicates the M_w 6.9 epicenter. The seventeen focal mechanisms obtained within the pre-October 25th 2018 sequence are colour-coded according to fault type (red=thrust, blue=normal, green=strike-slip). Locations i-iv indicate prominent earthquake clusters (see text for discussion). Z=Zakynthos Island. Bathymetry derives from https://www.gmrt.org/.

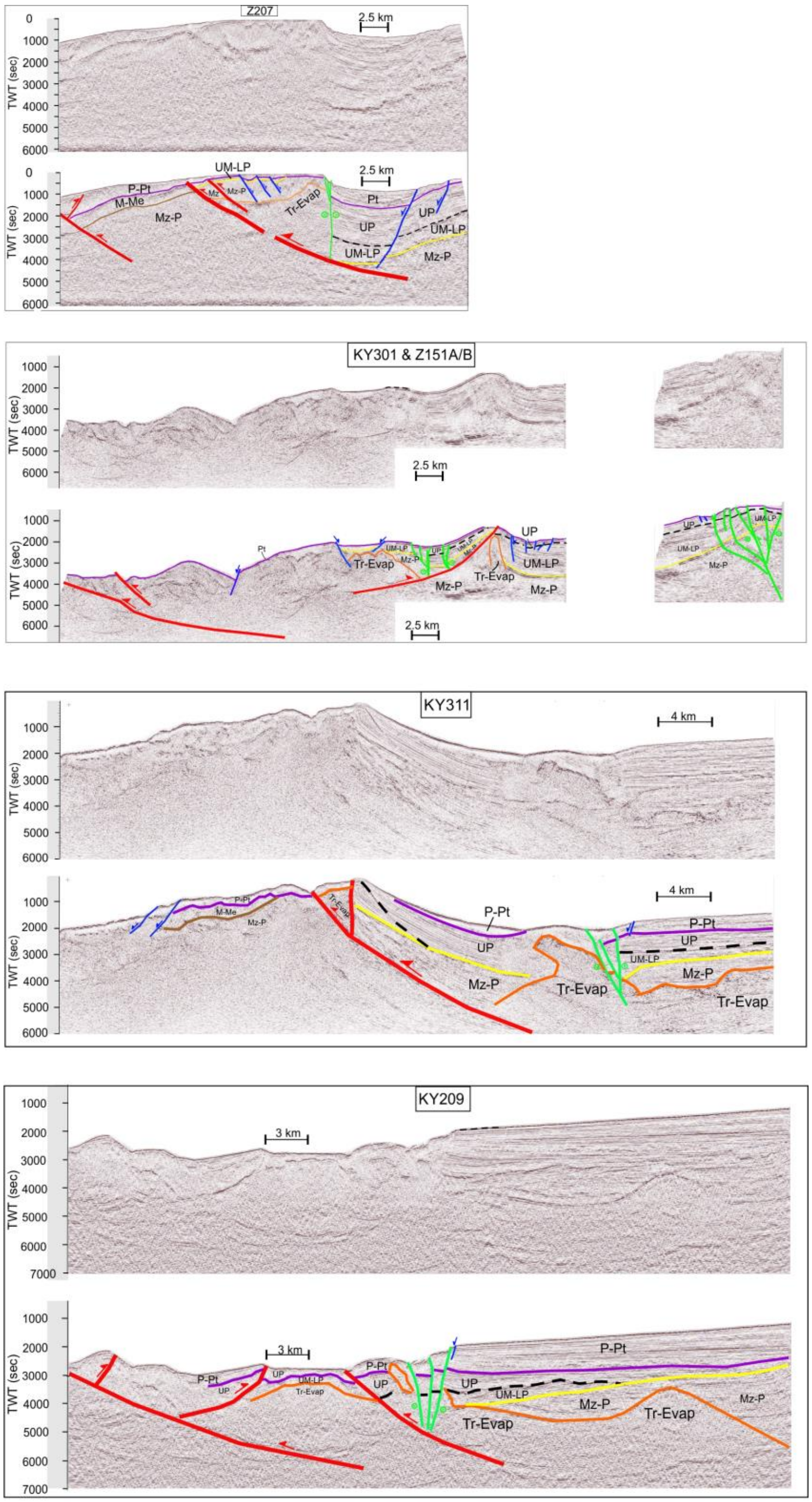

Figure 4. Long-term faulting and kinematics within the ZES. Migrated (top) and re-interpreted (bottom) sections of MCS seismic-reflection profiles Z207, KY301-Z151A/B, KY311 and KY209 from Wardell et al. (2014). Normal (blue), thrust (red) and strike-slip (green) faults are colour-coded as per focal mechanisms presented in Figures 3 and 5. P-Pt=Pliocene-Pleistocene, UP=Upper Pliocene, UM-LP=Upper Miocene-Lower Pliocene, M-Me=Miocene and Messinian, Mz-P=Mesozoic-Paleocene, Tr-Evap= Triassic evaporates (orange). The seismic stratigraphy is adopted from Kokalas et al. (2013).

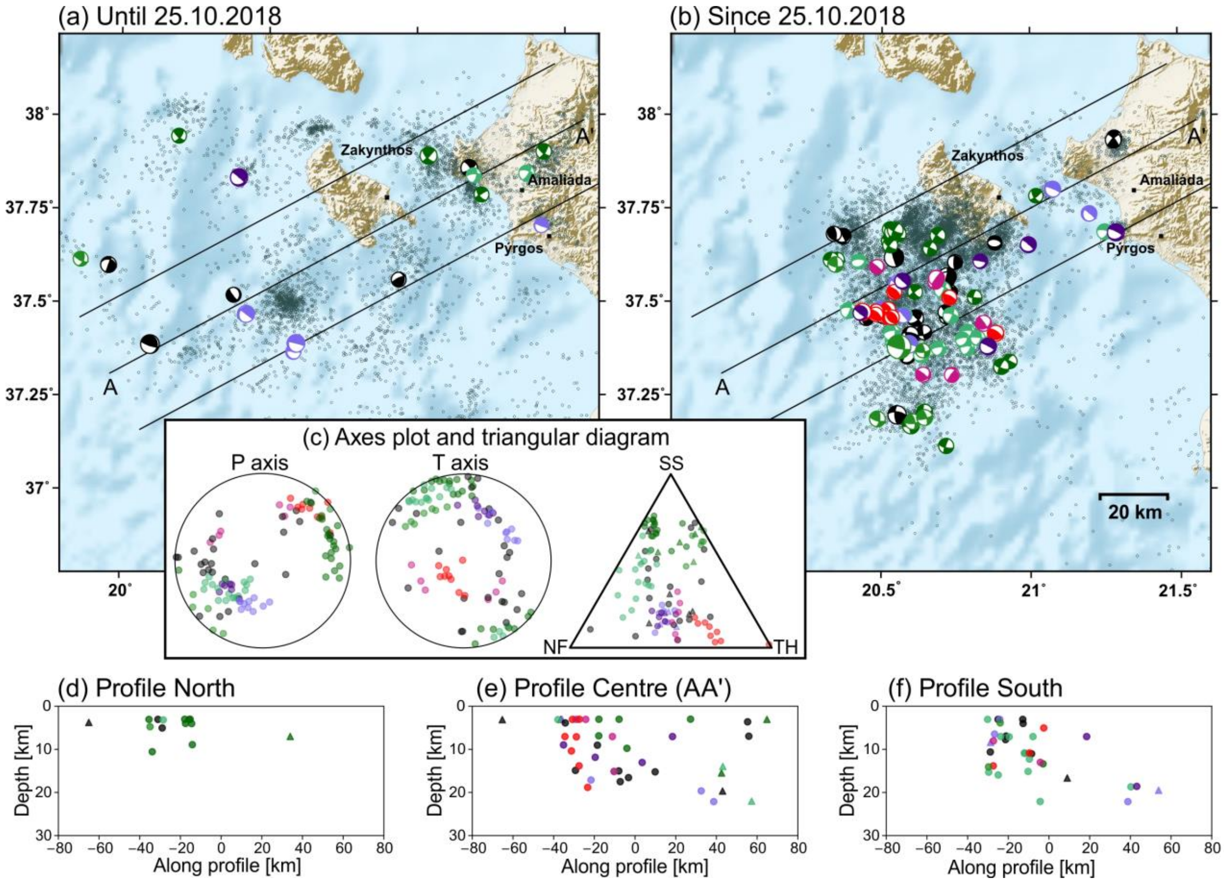

Figure 5. Focal mechanisms within the ZES. Map-view (a-b) and cross-sections (d-f) of 102 focal mechanisms from the ZES. Beachballs are colour coded according to 8 clusters of earthquakes with similar focal mechanisms, with the colours recalling the fault type (red=thrust, blue=normal, green=strike-slip and associated shadings when events span various types of faulting; black is used for solutions with unclustered focal mechanisms; see Supplementary Fig. S5 for details). The triangle diagram in (c) denotes the kinematics of events analysed by means of pressure (P) and tension (T) axes orientations and a triangular diagram after Frohlich (1992). Circles in c-f indicate events that occurred during the aftershock sequence while triangles represent events that occurred prior to the main event (Oct. 25th, 2018). The relocated ZES seismicity is indicated in (a) and (b) with small grey circles.

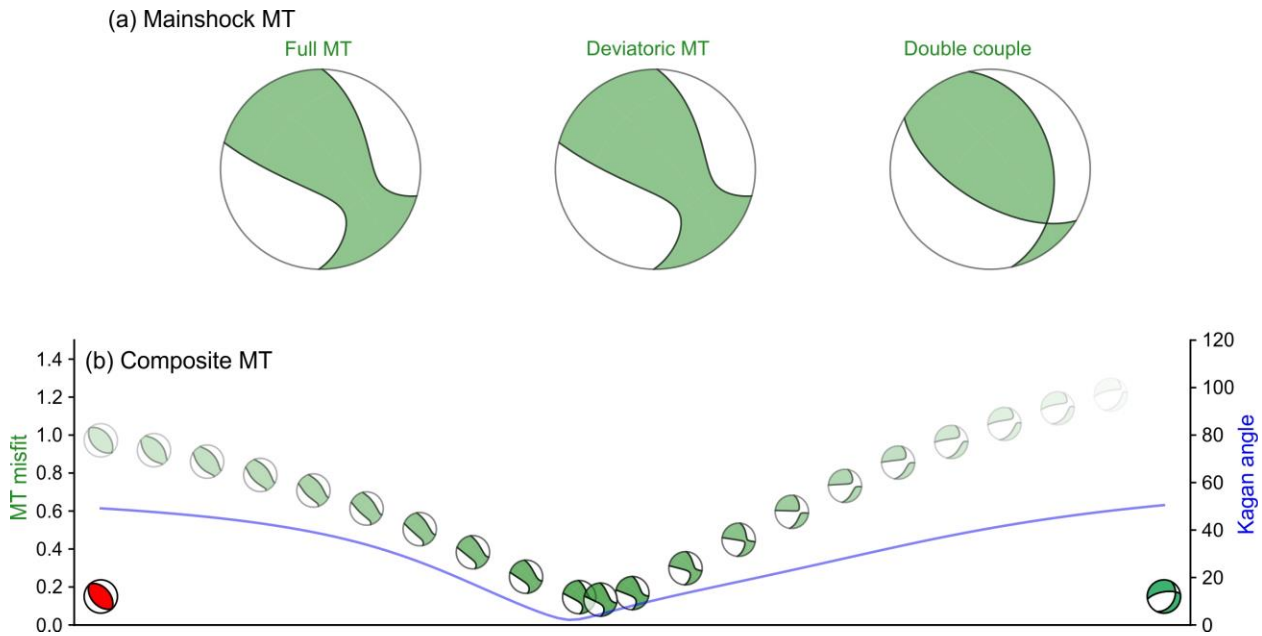

Figure 6. Mainshock moment tensor obtained (a) Full moment tensor (MT) obtained for the mainshock and its deviatoric and pure double couple (DC) components. (b) Overview of composite mainshock moment tensor obtained superposing two moment tensors with different contributions, one for an earthquake (5.11.2018 12:21) of the red thrust cluster and one for an earthquake (18.11.2018 5:18) of the sea-green cluster; focal sphere are plotted with lower transparency as they better fit the mainshock full MT (a blue line, denoting the Kagan angle among double couples of the mainshock and composite MTs, shows that the DC is also well reproduced for the suggested MT composition).

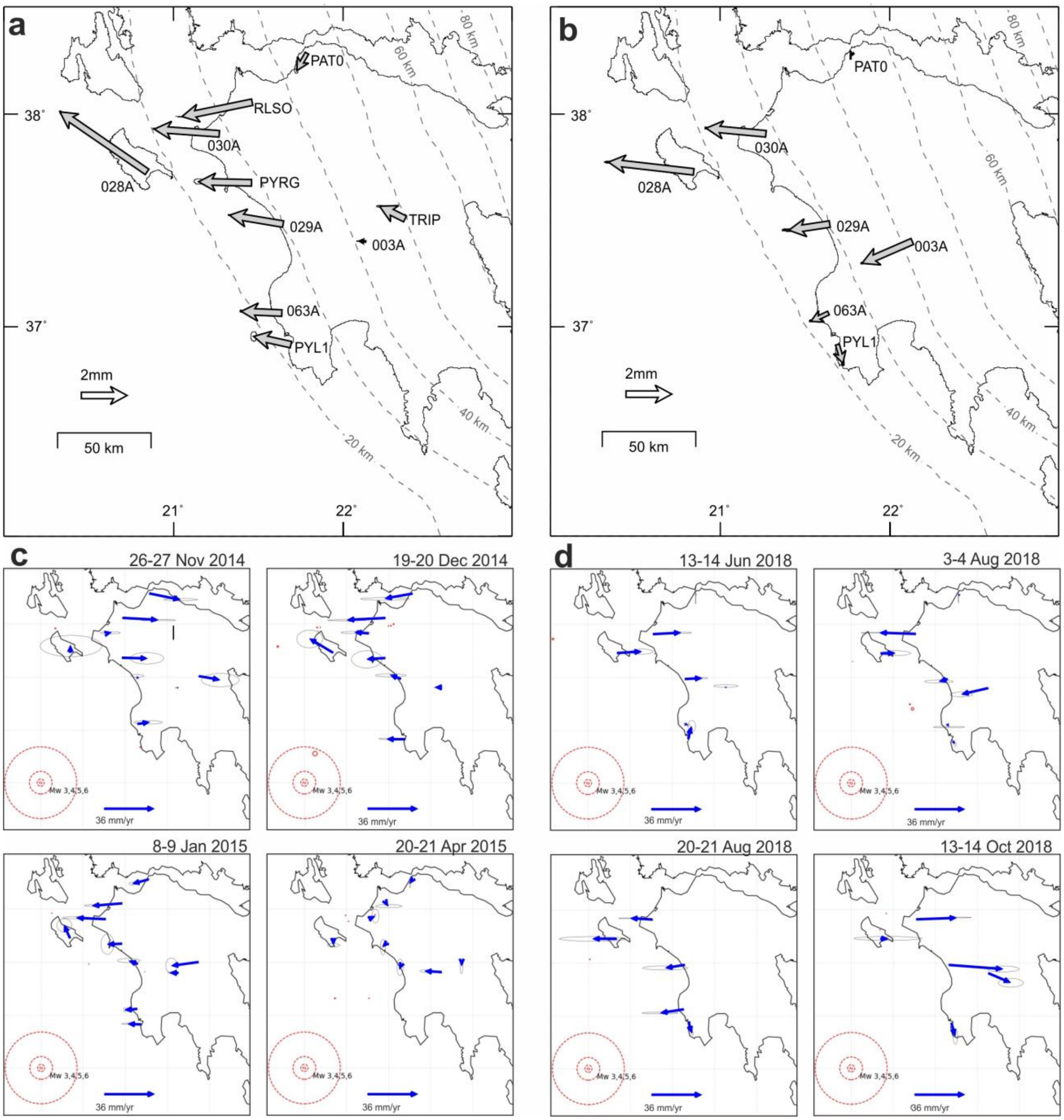

Figure 7. Slow-slip events along the termination of the HSS. Transient signals of surface deformation as derived from the analysis of GPS timeseries. Cumulative trench-ward transient displacements, together with their uncertainties (1-sigma), observed between **a,** 24.09.2014-20.03.2015 and **b,** 14.05.2018-25.10.2018 **c,** and **d,** Snapshots of the daily velocity evolution of the transient GPS signal with respect to the long-term velocity of each station for the periods corresponding to transient signals of (c) and (d), respectively. The upper-left panels in (c) and (d) show the network-wide acceleration observed before the reversal of the velocity vectors (Fig. 2e). Contours in a-b mark the top of the plate-interface (Halpaap et al., 2019).

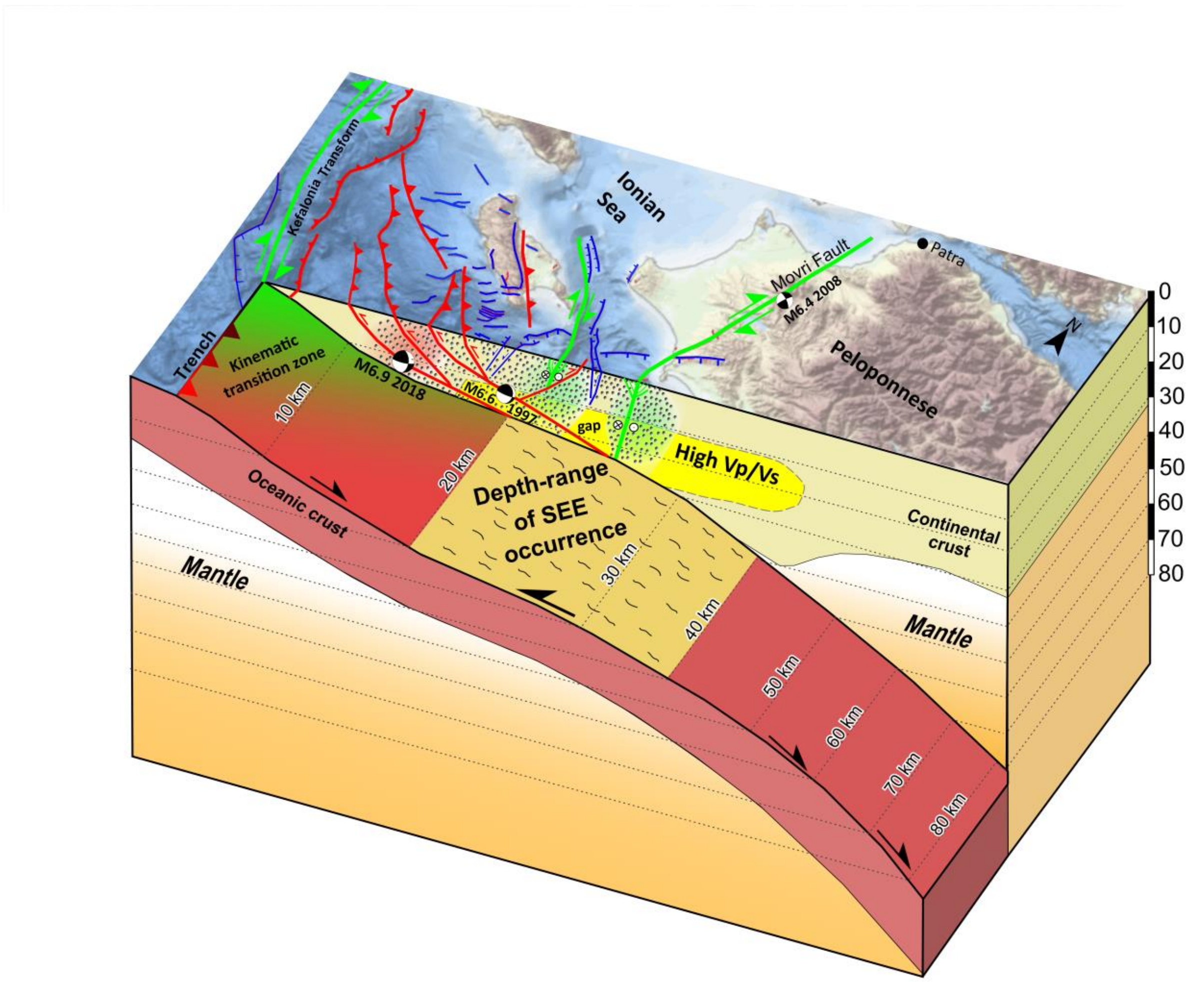

Figure 8. 3D-views of the deformation processes operating at the HSS termination. Schematic block diagram illustrating the spatial distribution of the seismic (earthquake) and aseismic (SSEs) deformation at the western-end of the Hellenic subduction margin as recorded during the 5 years preceding the M_w 6.9 Zakynthos Earthquake. Faults are colour-coded according to fault type (red=thrust, blue=normal, green= strike-slip) as per Figs 1, 3 and 4. The high Vp/Vs zone and the plate-interface contours derive from Halpaap et al. (2019). Shading around earthquakes highlights the larger clusters. The cross-section presented here partly reflects the seismic-reflection line KY301-Z151A/B presented in Figure 4 (for location see Fig. 1). The black moment tensor solutions indicate the two M>6 earthquakes that ruptured two distinct thrust faults of the study area (see caption of Fig. 1 for details). Offshore bathymetry derived from EMODnet (https://portal.emodnet-bathymetry.eu/?menu=19).